typeset using JPSJ.sty <ver.1.0b>

Longitudinal Structure Functions in Decaying and Forced Turbulence

Daigen FUKAYAMA[1] *, Toshihiro OYAMADA[1], Tohru NAKANO[1],
Toshiyuki GOTOH[2] and Kiyoshi YAMAMOTO[3]

[1] *Department of Physics, Chuo University, Tokyo 112-8551*
[2] *Department of Systems Engineering, Nagoya Institute of Technology, Nagoya 466-8555*
[3] *National Aerospace Laboratory, Chofu, Tokyo 182-8522*

(Received)

In order to reliably compute the longitudinal structure functions in decaying and forced turbulence, local isotropy is examined with the aid of the isotropic expression of the incompressible conditions for the second and third order structure functions. Furthermore, the Karman-Howarth-Kolmogorov relation is investigated to examine the effects of external forcing and temporally decreasing of the second order structure function. On the basis of these investigations, the scaling range and exponents ζ_n of the longitudinal structure functions are determined for decaying and forced turbulence with the aid of the extended-self-similarity (ESS) method. We find that ζ_n's are smaller, for $n \geq 4$, in decaying turbulence than in forced turbulence. The reasons for this discrepancy are discussed. Analysis of the local slopes of the structure functions is used to justify the ESS method.

KEYWORDS: Karman-Howarth-Kolmogorov equation, isotropy, external forcing, non-stationarity, structure functions, longitudinal velocity increment

§1. Introduction

Study of structure function is useful in the analysis of the scaling property of fully-developed turbulence.[1)] In particular, the structure function of the longitudinal velocity increment clearly shows how the scaling deviates from K41 scaling[2)] as the order of the structure function increases.[3)] The structure function of a transverse velocity increment also exhibits deviation from K41 scaling, but the values of the scaling exponents appear to differ from those of the longitudinal variety, reflecting the influence of vortical structures in turbulence.[4, 7, 5, 8, 9, 6)]

All measurements in direct numerical simulations (DNS's) and experiments include certain limitations or restrictions. Examples of these restrictions are the limitation of the Reynolds number to finite values, the size of the samples, and the degree of deviation from isotropy, homogeneity, and stationarity that are allowed to the system. Therefore the results obtained from such data must be studied carefully and thoughtfully. To be more specific, consider the DNS of forced homogeneous isotropic turbulence with a finite Reynolds number, in which the random forces are assumed to be statistically homogeneous, isotropic and Gaussian with a given spectrum. In order to realize a high Reynolds turbulence number, the force spectrum is assumed to have compact support at the very low wavenumber range, $1 \leq k \leq 2 \sim 3$. This restriction introduces a problem of convergence to large scale values with respect to isotropy, homogeneity and stationarity. Since the small number of Fourier modes in the forced band have a large amount of kinetic energy, and their characteristic times are long, fluctuation of these modes significantly affects the statistics of large-scale turbulence, which possibly pertain to the inertial region. The difficulty lies in determining for how long statistical quantities must be averaged to assure statistical homogeneity, isotropy and stationarity of the system, and in discovering the largest scale not affected by the external forces.

In simulation of decaying turbulence, similar problems arise, because the fluctuations of the Fourier modes in the lower band are large at $t = 0$. Hence the issues to be addressed are the effect of non-stationarity on the intensity of fluctuations, the anisotropic effect due to large eddies, and the size of the largest scale that is not influenced by a decrease in the intensity of fluctuations.

In laboratory tests, such as experiments using the turbulence in a cylinder with disks rotating in opposite directions,[10)] we find a situation similar to the case of forced DNS. The geometry of the experimental apparatus imposes certain limitations on the isotropy and homogeneity of the system, although the sample size is relatively larger than in the DNS case and the Reynolds number is relatively lower than that in the case of atmospheric flow. Also, the total record length is usually much longer than the large-eddy turnover-time. In an atmospheric flow, on the other hand, the Reynolds number is usually very large, but the characteristic time of the macroscale shear quite often becomes comparable to or longer than the record length. Thus, the homogeneity and isotropy conditions are not well satisfied, and the problem of statistical convergence at large scales arises.[6)]

Most studies of the scaling of structure functions in the DNS have been made using a very limited number of samples, and the results may therefore suffer from the effects discussed above. Hence, there are several factors to be checked before drawing definite conclusions from simulations about scaling; they are: (1) the degree of

* E-mail address: daigen@phys.chuo-u.ac.jp

isotropy of turbulence in the scaling region, (2) the effect of external forcing, and (3) the effect of decreasing intensity of fluctuations. Forced simulation cannot avoid the first two factors, while the first and third factors are crucial in decaying simulation. Thus, we need to investigate the effects of limiting the Reynolds number to finite values, and then determine the resulting longitudinal structure function.

In the present paper we carefully examine the above three factors in decaying and forced simulated turbulence with various Reynolds numbers. In particular, flows of Reynolds number $R_\lambda = 70$ are carefully studied. Twelve decaying turbulences with the same initial energy spectrum (but different realizations) are simulated, and the forced turbulence is executed for a long period of time, providing an average over 126 samples, during approximately 50 eddy turnover times. The degree of local isotropy is studied through the incompressible-condition restriction on the second and third order structure functions. How external forces penetrate into the upper inertial region in forced turbulence and how the nonstationarity of the fluctuations deteriorates the upper inertial region in decaying turbulence are investigated through the Karman-Howarth-Kolmogorov relation (referred to as the KHK relation hereafter).[11] The KHK relation is an exact expression connecting the third-order structure function to the second order structure function. On the basis of these studies, we estimate the scaling exponents of the longitudinal velocity structure functions in forced and decaying turbulence by employing the extended-self-similarity (ESS) method.[12,13] We find that the scaling exponents of the forced turbulence agree with other currently reported values,[3] but that the scaling exponents of decaying turbulence are smaller for higher orders than the corresponding exponents of steady turbulence. A reason for this behavior is suggested using the equation for the structure function of arbitrary order, which is a generalization of the third-order structure function.

Our paper is organized as follows. In section 2, the relevant data from several simulations of decaying and forced turbulence are summarized. Section 3 is devoted to discussion of the isotropy of turbulence, while the KHK relation is investigated in section 4. In section 5 the longitudinal structure function is obtained in the scale range that is appropriate for the KHK relation and the conditions of isotropy to hold. The scaling exponents of longitudinal structure functions up to the eighth order are derived using the ESS method. Evidence that the exponents for decaying turbulence are smaller than those for forced turbulence is also presented. In section 6, the effect of the finite Reynolds number on the structure of the local exponents is discussed, and a justification for the ESS method is given. In the appendices, the equation for the structure function of arbitrary order is derived and, in particular, the second-order equation is shown to reduce to the KHK relation. Additionally, the contribution of the pressure gradient term in the equation for the structure function is shown to be short ranged.[14]

	Run 1	Run 2	Run 3	Run 4	Run 5
condition	decay	decay	decay	forced	forced
mesh points	256^3	256^3	512^3	256^3	512^3
R_λ	70	90	120	70	125
$k_{\max}\eta$	1.11	1.26	1.42	2.32	2.03
N	12	1	1	126	45

Table I. Various parameters in decaying and forced simulations. N is the number of samples over which the average is taken.

§2. Numerical Procedure

Three kinds of decaying runs were carried out for the Gaussian, random, initial-velocity field, using the same energy spectrum $E(k,0) = c(k/k_0)^4 \exp[-2(k/k_0)^2]$($k_0 =$ 3 for Run 1 and $k_0 = 1$ for Run 2 and Run 3), but with different realizations. The number of mesh points used were 256^3 for Runs 1 and 2, and 512^3 for Run 3. Run 1 consisted of 12 different sub-runs with the same Reynolds number. The numerical algorithm used for the calculations is the pseudo-spectral method in space, and the fourth-order Runge-Kutta-Gill method in time. Aliasing errors were eliminated through application of the shift method. The computations were carried out on a parallel vector-machine at NAL's Numerical Wind Tunnel and at RIKEN's Advanced Computing Center. The various data were taken at the time where the energy dissipation had reached the maximum value. The relevant data are shown in Table I. The spatial resolution of the DNS's may be estimated by the value of the product $k_{\max}\eta$, where η is the Kolmogorov length. For all runs, the values obtained are larger than unity, implying that sufficient resolution was obtained for even the smallest scale.

The numerical method used for forced turbulence is essentially the same as that used for decaying turbulence. The initial conditions applied to the forced-turbulence experiment were also the same as those used in the decaying-turbulence test. The random force is statistically homogeneous, isotropic and Gaussian white, and its spectrum support is limited to the band $2 \lesssim k \lesssim 3$. Also, the spectrum form is constant in the band. The data are shown in Table I. After the transient period had passed, usually after a few turnover times, steady states were attained and the time average was computed over some multiple of the turnover time. For example, Run 4 was averaged over 126 samples during 50 eddy turnover times, and Run 5 was averaged over 45 samples during 9 eddy turnover times. The computations were performed at RIKEN's Advanced Computing Center.

§3. Isotropy

There are many ways to check the isotropy of turbulence. One is to examine the relation $\langle u^2 \rangle = \langle v^2 \rangle = \langle w^2 \rangle$, which reflects the isotropy of the largest scale, or the 'global" isotropy. In order to check the degree of local isotropy of eddies of scale r, which is necessary to compute the scaling exponents of the structure functions, we study the isotropic nature of the second and third

order structure functions. When the incompressible condition is applied to the second and third order structure functions, the following relations result for the isotropic case:[1)]

$$D_{TT}(r) = D_{LL}(r) + \frac{r}{2}\frac{\mathrm{d}D_{LL}(r)}{\mathrm{d}r}, \tag{3.1}$$

$$D_{LTT}(r) = \frac{1}{6}\frac{\mathrm{d}}{\mathrm{d}r} r D_{LLL}(r), \tag{3.2}$$

where $D_{LL} \equiv \left\langle (\delta u_l)^2 \right\rangle$, $D_{TT} \equiv \left\langle (\delta u_t)^2 \right\rangle$, $D_{LLL} \equiv \left\langle (\delta u_l)^3 \right\rangle$, $D_{LTT} \equiv \left\langle \delta u_l (\delta u_t)^2 \right\rangle$, δu_l is the longitudinal velocity increment over a distance r, and δu_t is the transversal velocity increment. Instead of the differential forms shown above, in the following derivations we employ the integral forms

$$\int_0^r \left(D_{TT}(r') - \frac{1}{2} D_{LL}(r') \right) \mathrm{d}r' = \frac{1}{2} r D_{LL}(r), \tag{3.3}$$

$$\int_0^r D_{LTT}(r') \mathrm{d}r' = \frac{1}{6} r D_{LLL}(r), \tag{3.4}$$

because numerical computation is less noisy for the integrals than for the derivatives.

3.1 Decaying turbulence

Figures 1(a) and 1(b) show comparisons with varying r for Run 1, averaged over 12 samples of different realizations. This shows that the above relations are satisfied. The relation (3.4) for the third-order structure function is less accurate than that for the second-order, but it still holds up to $r_* \equiv r/\eta = 160$. (Note that from now on, the scale r will be expressed in units of the Kolmogorov length η.) The local isotropy of the structure functions is improved with an increase in the number of samples. To witness this, consider the isotropic relation for Run 2, consisting of a single sample. In this case, the third-order relation was found to be slightly violated beyond $r_* = 30$ (figures not shown).

Later we will determine the scaling indices of the longitudinal structure functions in the inertial range using the ESS method. We will employ the scale range $16.0 \le r_* \le 29.4$ for Run 1. Because of this choice of scale range, the structure functions in the inertial region are not affected by any lack of accuracy in the degree of the isotropic condition of the turbulence. This is the case for Runs 2 and 3.

Although it is not as easy to check the isotropy of the higher-order structure functions as it is to check the second and third-order functions, we expect the statistical convergence for the isotropy of the structure functions to be gradually lost as the order of the function increases. This is because the higher-order structure functions are dominated by rare, strong events that are oriented in specific directions. However, this does not necessarily mean that the degree of anisotropy of the fourth-order structure function is larger than that of the third-order structure function. The statistical convergence of even-ordered structure functions is faster than that of odd-ordered structure functions.

In decaying turbulence, the state of isotropy is satisfactorily established. Although a sufficient number of samples is desirable for computation of the structure functions, the data of a single snap-shot (as in Run 2 or 3) are enough to determine the structure functions with respect to the degree of isotropy. This, however, is not the case with forced turbulence, as is discussed below.

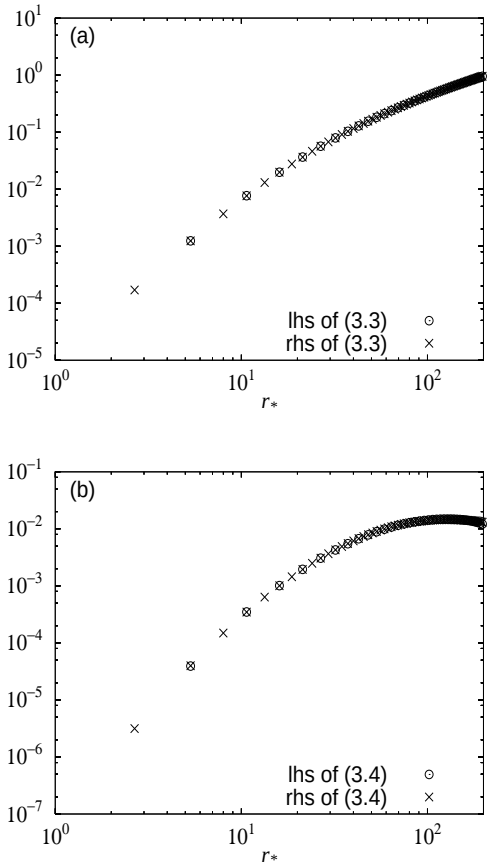

Fig. 1. The isotropic conditions for Run 1, consisting of 12 identical samples with different realizations. (a) The second-order structure function; (b) the third-order structure function.

3.2 Forced turbulence

It is important to note that the conditions (3.3) and (3.4) are not satisfied for forced turbulence as well as they are for decaying turbulence, particularly when the data of only one snap shot are processed. To see this explicitly, we show in Figs. 2(a) and 2(b) the curves of eqs. (3.3) and (3.4) for Run 4 at a certain instant after the turbulence reaches the steady state. Although the second-order structure function satisfies the isotropic condition, the same condition applied to the third-order structure function is violated at all scales. This indicates that an average over a prolonged period is needed to establish the degree of isotropy for forced turbulence. On the other hand, Figs. 3(a) and 3(b) show curves for Run 4 averaged over 126 samples, with the averaging-time being approximately 50 eddy turn-over times. The isotropy condition for the second-order structure function is thus ensured quite satisfactorily. The isotropy condition for the third-order structure function, however, is only satisfied up to $r_* = 50$. We expect that the condition for statistical isotropy becomes better satisfied as the num-

ber of samples increases, and as the averaging-time increases. This would suggest that steady turbulence with isotropic forcing needs to be studied over a sufficiently prolonged averaging time.

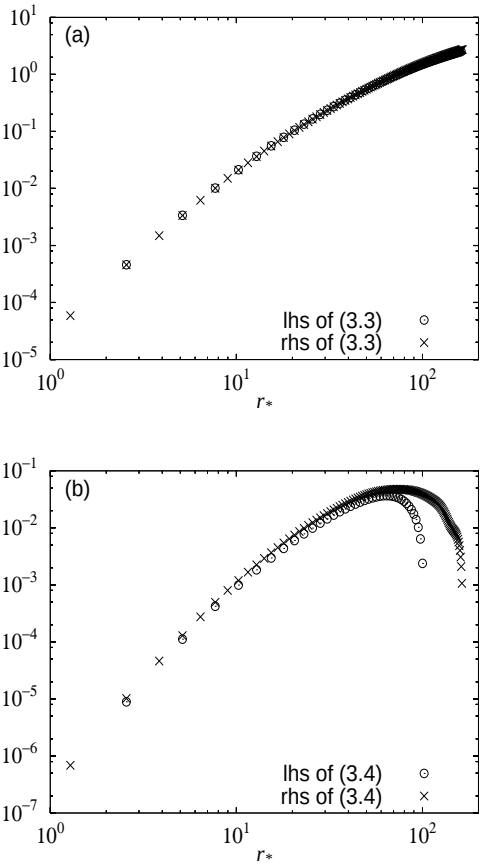

Fig. 2. The isotropic conditions at one snap-shot for Run 4, when the energy dissipation reaches a constant level. (a) The second-order structure function; (b) the third-order structure function.

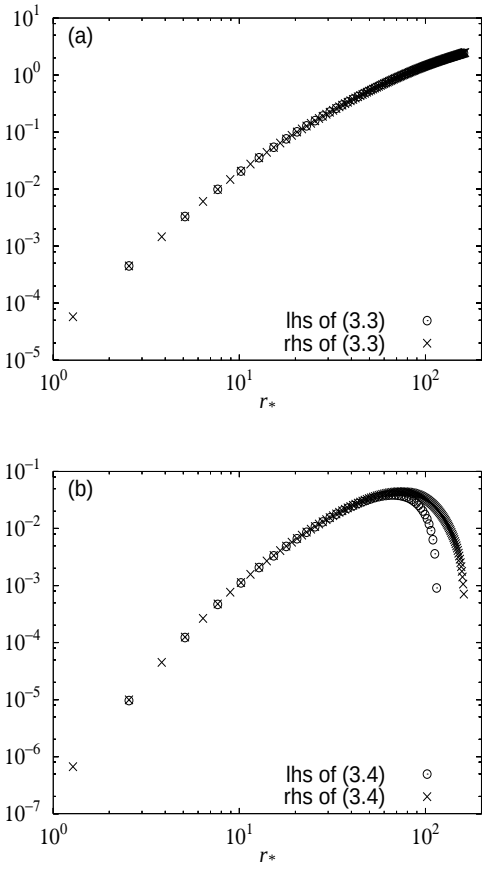

Fig. 3. The isotropic conditions for Run 4 averaged over 126 samples during approximately 50 eddy-turnover times. (a) The second-order structure function; (b) the third-order structure function.

§4. The Karman-Howarth-Kolmogorov Equation

In this section we consider, through the KHK relation,[11] how external forcing (in forced turbulence) and non-stationarity of the intensity of fluctuations (in decaying turbulence) affect the transfer of energy in scale-space. The effects of the external forcing and non-stationarity on a weighted transfer of energy, which is the average of the product of the energy-dissipation rate and the multiples of the velocity-increment, associated with the higher-order structure functions are discussed later.

The KHK relation is an exact equation, which is very rare in turbulence theory. The equation for the second-order structure function employing the isotropic condition is written:

$$D_{LLL}(r) = -\frac{4}{5}\overline{\varepsilon}r + 6\nu\frac{\partial D_{LL}}{\partial r} + G(r) + F(r), \qquad (4.1)$$

where

$$G(r) = -\frac{3}{r^4}\int_0^r \frac{\partial D_{LL}}{\partial t} r'^4 \mathrm{d}r', \qquad (4.2)$$

and

$$F(r) = \frac{2}{35}\varepsilon_{in}(k_e r)^2 r, \qquad (4.3)$$

as is derived in eq. (A·9) of Appendix A. Note that equation (4.1) is valid for decaying turbulence as well as for the forced variety. Here $\overline{\varepsilon}$ is the average dissipation rate, while ε_{in} is the energy input rate due to external random forces, which are distributed about $k \sim k_e$. Note that ν represents the kinematical viscosity. The second term on the right-hand side (RHS) of eq. (4.1) expresses the effect of viscous damping, while the third term on the RHS relates the effect of the non-stationarity (decreasing in time) of the second-order structure function, which is significant for decaying turbulence. The fourth term on the RHS expresses the effect of the external forces. Note that only in steady, forced turbulence does $\overline{\varepsilon} = \varepsilon_{in}$. It is of some interest to note that the first term on the RHS of eq. (4.1) is negative, while the viscous term, the external-forcing term and the non-stationarity term are positive.

In the inertial region of stationary-turbulence with infinite Reynolds number, one can neglect the second, third and fourth terms on the RHS of the above equation, so

that one gets Kolmogorov's well-known 4/5 law:[15)]

$$D_{LLL}(r) = -\frac{4}{5}\overline{\varepsilon}r. \tag{4.4}$$

The inertial region in real flows with finite Reynolds numbers is regarded as having the relation (4.4) hold approximately, and hence the universal scaling property of the structure functions in the inertial region must be examined only under these conditions. In actual flows, however, the Reynolds number is not large enough to guarantee the wide spatial range in which eq. (4.4) will hold.

For flows of finite Reynolds numbers, therefore, the important issue is how the transfer term $-(4/5)\overline{\varepsilon}r$ is affected by (1) the viscous damping term, (2) the non-stationarity term in decaying turbulence and (3) the external forcing term in forced turbulence. Case (1) is significant in the lower inertial region, while (2) and (3) are pertinent in the upper inertial region. We investigate each term in the KHK equation for both the decaying- and forced-turbulence scenarios. The failure of eq. (4.1) is caused by the breakdown of the isotropic condition, and by the insufficient number of samples averaged.

Now, concerning the numerical computation, $\overline{\varepsilon}$ was calculated from the square of the spatial derivative of the velocity field, while the forcing term $F(r)$ in eq. (4.3) was computed with the aid of the spectrum of the random forces, not from an external energy input at each instant. More precisely, we did not use the approximation $F(r)$ for the forcing term, but the exact expression (A·10) in Appendix A; we did this because, in this case, $k_e r$ is not limited to $k_e r \ll 1$. The other terms in the expression are all evaluated directly through processing the data.

4.1 Decaying turbulence

The Karman-Howarth-Kolmogorov relation now takes the form

$$D_{LLL}(r) = -\frac{4}{5}\overline{\varepsilon}r + 6\nu\frac{\partial D_{LL}(r)}{\partial r} + G(r). \tag{4.5}$$

In Fig. 4, we depict $-D_{LLL}(r)/\overline{\varepsilon}$ and the combined sums of the terms on the right-hand side of eq. (4.5) divided by $\overline{\varepsilon}$, against the scale r_* for Run 1 (averaged over 12 samples.) The relation (4.5) is well satisfied for all values of r_*.

From Fig. 4 it can be seen that the peak of $-D_{LLL}(r)/(\overline{\varepsilon}r)$ is 0.53 at $r_* = 26.7$, and the linear region of $D_{LLL}(r)$ is extremely narrow around $r_* \sim 23$. If the viscous effect is included, however, $-D_{LLL}(r) + 6\nu\partial D_{LL}/\partial r$ is in near-agreement with $(4/5)\overline{\varepsilon}r$ up to $r_* = 10$. If the non-stationarity of D_{LL} is taken into account, agreement is guaranteed for any scale. The effect of the non-stationarity of D_{LL} becomes more significant as the separation scale r increases, indicating that the amplitudes of larger-scale components decay faster than those of smaller-scale components. This is because the former do not have any energy supplied to them in the decaying turbulence. The non-stationarity term, which has been included in Fig. 4, is observed to decrease as r^c for $5 \le r_* \le 30$, and where c is almost 3. This constant slope is surprising, because the scaling range of the non-stationarity term extends from the inertial to the dissipation region.

We will now discuss the form of the KHK relation in connection with the structure function, with the details of the computations shown in the following section. As seen from Fig. 4, corresponding to Run 1, it is difficult to find the region where $D_{LLL}(r) = -(4/5)\overline{\varepsilon}r$. This implies that computation of the exponents in the inertial region by the direct-fitting method is not possible. We therefore employ the ESS method[12, 13)] to calculate the scaling exponents of the structure functions. The ESS method is known to extend the scaling region down to the upper dissipation range,[16)] because the third-order structure function used in the abscissa contains the effect of the viscous-damping term. In the following section, on the other hand, we will show that the ESS method yields reasonable values beyond $r_* = 20$ up to $r_* = 30$, where, as Fig. 4 shows, the non-stationarity effect cannot be neglected. Thus the ESS method extends the scaling region upward in the scale-space in decaying turbulence.

The KHK equation has been experimentally investigated in grid-turbulence by Danaila *et al.*,[17)] who took into account the non-stationarity term by approximating it using spatial differentiation under the Taylor hypothesis. They claimed that the KHK equation is correct up to $r_* \sim 200$; however a slight discrepancy is seen around $r_* \sim 20$ (Fig. 3 in ref. 17). Such a deviation negatively influences the determination of the scaling exponents of the higher-order structure functions. The non-stationarity term takes the form r^c with $1 < c < 2$, in contrast to our assumed value of $c = 3$. The reason for this discrepancy is not currently known.

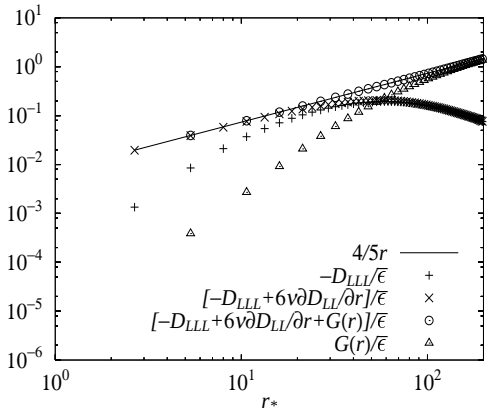

Fig. 4. The KHK relation for decaying turbulence for Run 1 averaged over 12 samples.

4.2 Forced turbulence

In this case the KHK equation takes the form

$$D_{LLL}(r) = -\frac{4}{5}\overline{\varepsilon}r + 6\nu\frac{\partial D_{LL}(r)}{\partial r} + F(r), \tag{4.6}$$

where the last term is numerically computed with the help of the exact expression (A·10) in Appendix A. It is interesting to note that the relation (4.6) does not hold

when the data of only a single instantaneous snap-shot are processed. This situation is analogous to having the isotropic condition fail in Fig. 2. The reason for the similarity is that both are linked to a random feature in the external input. The last term in eq. (4.6) is calculated using an ensemble-average value from the spectrum of $\langle |f_i(\boldsymbol{k})|^2 \rangle$, which is equivalent to a time average over a sufficiently long period. Let us now estimate how the input term varies from time to time. The number of input modes is $N = 160$ for Runs 4 and 5, so that a simple estimate of the relative amplitude of the input fluctuation is of the order $1/\sqrt{N} \sim 0.1$. This implies that the external-forcing term at any given instant may have a relative error on the order of 10%. In order to obtain reliability of the forcing term to within a 1% error, we need 10^4 random forces, which corresponds to roughly one eddy-turnover time in our present simulation. To obtain the statistically meaningful result of eq. (4.6) we require a much longer averaging period than over only one eddy-turnover time.

Figure 5 displays the KHK curve for Run 4 with its average over 126 samples, in a time interval of roughly 50 eddy-turnover times. It is not surprising that the KHK relation holds here for almost any separation, since the relation is exact under the isotropic condition. Let us now inspect the contribution of each term in the KHK equation to its total value. According to Fig. 5, the peak of $-D_{LLL}(r)/(\overline{\varepsilon} r)$ is 0.58 at $r_* = 26.8$, and the flat region of $D_{LLL}(r)/r$ is extremely narrow around $r_* \sim 26$. This is very similar to the situation encountered in the decaying turbulence studied in Run 1. If the viscous effect is also taken into account however, the agreement of $-D_{LLL}(r) + 6\nu\partial D_{LL}/\partial r$ with $(4/5)\overline{\varepsilon} r$ is nearly correct up to $r_* = 20$. If the effect due to external forces is included, which begins to appear at $r_* \sim 20$, the agreement between the two relations is perfect.

Also of interest are the results of Run 5, averaged over 45 samples, during nine eddy-turnover times. Here the KHK relation is not obeyed as well as in Run 4. Our computations confirm that agreement improves as the sample number increases, which explains why the agreement is better for Run 4. Note however that the improvement in agreement is small with modest increases in sample number.

The KHK relation for a real flow was recently studied[10] for low temperature helium gas flows, with R_λ ranging from 120 to 1200, using an apparatus in which the turbulence is forced by two counter-rotating disks in a cylindrical container. The effects of large-scale motions were included in eq. (4.6) as the external-forcing term. The exact nature of eq. (4.6) was proved in this experiment, except for large scales, where non-isotropic forcing has a dominant effect.

§5. Longitudinal Structure Functions

Let us begin with an estimate of the maximum degree of the order of structure functions that we desire to measure accurately. We plot the probability-density function $P(u_r)$ multiplied by u_r^n against u_r, where u_r is the longitudinal-velocity increment over the distance r.

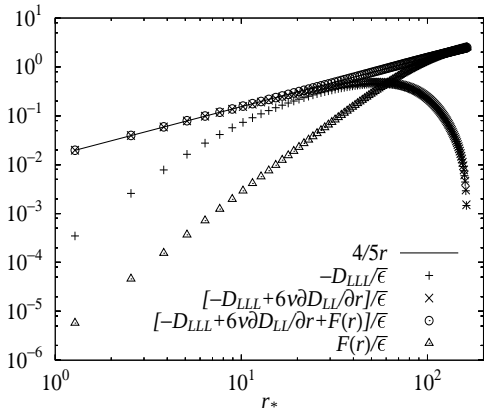

Fig. 5. The KHK relation for Run 4 averaged over 126 samples.

As n increases, the peak of the bell shape of $u_r^n P(u_r)$ approaches the larger value of $|u_r|$. Beyond a certain value of n, the peak cannot be distinguished and rare strong events heavily influence the computation of $\langle u_r^n \rangle$. Figure 6 is an example of such a plot, showing $u_r^8 P(u_r)$ at $r_* = 20.8$ (Run 3). The abscissa in the plot is $u_r/\sqrt{S_2(r)}$, while the ordinate is pre-divided by $S_2(r)^4$. The curves decay quickly for large amplitudes. For the plots of $u_r^n P(u_r)$ with $n \geq 9$, we observed that the decay of the curves is not sufficiently fast to ensure that moments higher than the ninth order are computed accurately (figure not shown). Thus we conclude from these simulations that $n = 8$ is the maximum order allowed for the condition of a sufficient-number-of-events to be met in the statistical sense.

In this paper we will concentrate our efforts only on the study of the longitudinal-velocity structure function

$$S_n(r) = \langle u_r^n \rangle. \tag{5.1}$$

Before going on to determine the exponents of $S_n(r)$, we will examine the structure functions of odd orders. For this purpose, let us recall the probability-density function (PDF) of u_r: $P(u_r)$. The peak of the PDF is located at the small positive value of u_r, while its tail is more populated on the negative side than on the positive side, in accordance with $\langle u_r \rangle = \int u_r P(u_r) \mathrm{d}u_r = 0$. For $\langle u_r^3 \rangle$, on the other hand, the contribution from the negative values of u_r is larger than that from the positive values, implying a negative value for $S_3(r)$. Note that $S_n(r)$ becomes more negative as the odd values of n increase. Since the structure function of odd order is determined from the difference of two terms of almost equal magnitude, contributed from positive and negative values of u_r, a delicate balance between the two terms is responsible for the behavior of the odd-order structure functions. The structure functions of even order are the sum of those same terms, and do not rely on that intricate balance. Thus reliable evaluation of the odd-ordered structure functions is more difficult than evaluation of the even-ordered structure functions, and a smooth change in the exponents of $S_n(r)$ with respect to varying r in n, is expected only for flows of extremely large Reynolds number. A way of overcoming this difficulty for moderate Reynolds numbers is to employ the generalized structure

functions $\langle |u_r|^n \rangle$ instead of $S_n(r)$.[4,5,6,13,18,19,20,21] We thus introduce

$$\tilde{S}_n(r) = \langle |u_r|^n \rangle. \tag{5.2}$$

$\tilde{S}_n(r)$ will now reflect the change of the entire form of PDF, with respect to u_r, so that the scaling exponents of $\tilde{S}_n(r)$ are now expected to vary smoothly with n. It is expected that the exponents of $S_n(r)$ and $\tilde{S}_n(r)$ for an odd number of n will be identical for large Reynolds numbers. In what follows, we drop the symbol tilde on S_n so that no confusion will result.

When we plot $S_n(r)$ against r_*, it is difficult to read the exponent ζ_n defined in the relationship

$$S_n(r) \sim r^{\zeta_n}. \tag{5.3}$$

An example of this is shown in Fig. 7, where curves of $S_6(r)$ for Run 1 (decaying turbulence, 12 samples) and for Run 4 (forced turbulence, 126 samples) are plotted against r_*. The magnitude of both these quantities changes in such a way that both curves agree with each other in the dissipative region. It should be noted that the slope of $S_6(r)$ for decaying turbulence (Run 1) is smaller than that of the same quantity for forced turbulence (Run 4). The local slope $\mathrm{d}\log S_6(r)/\mathrm{d}\log r$ never assumes a constant value over an extended range, as shown in Fig. 8. Often, for moderate Reynolds number flows, the ESS method[12,13] is used instead of the above direct method. Following the work of many authors ,[4,5,6,12,13,16,18,19,20,21] we have plotted $S_n(r) = \langle |u_r|^n \rangle$ against $S_3(r) = \langle |u_r|^3 \rangle$ instead of $\langle u_r^3 \rangle$, for the reason stated previously in this section. Figure 9 shows a plot of $S_6(r)$ against the $S_3(r)$ corresponding to Fig. 7; the power law tendency is clearly seen in this comparison.

The exponents of $S_n(r)$ are obtained from the graph of the local exponent of $\log S_n(r)$ against $\log S_3(r)$. Combining $S_n(r) \sim r^{\zeta_n}$ and $S_3(r) \sim r^{\zeta_3}$, we have

$$S_n(r) \sim S_3(r)^{\zeta_n/\zeta_3}. \tag{5.4}$$

Hence, the slope of the plot of $\log S_n(r)$ against $\log S_3(r)$ is $\zeta_n/\zeta_3 = \zeta_n$, since ζ_3 is assumed to be unity.

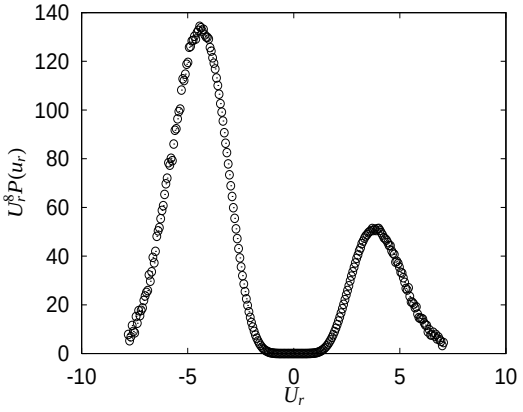

Fig. 6. The plot of $U_r^8 P(u_r)$ against U_r at $r_* = 20.8$ for Run 2, where $U_r = u_r/\sqrt{S_2(r)}$.

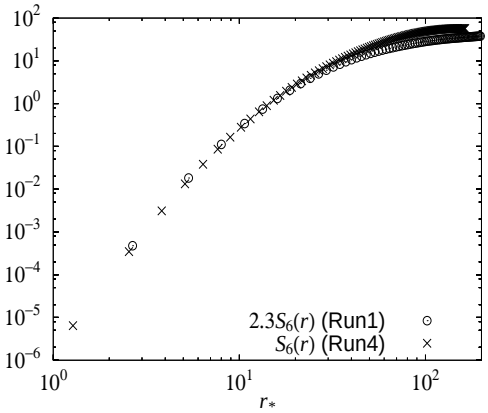

Fig. 7. The plot of $S_6(r)$ against r_* for Run 1 (decaying turbulence) and Run 4 (forced turbulence).

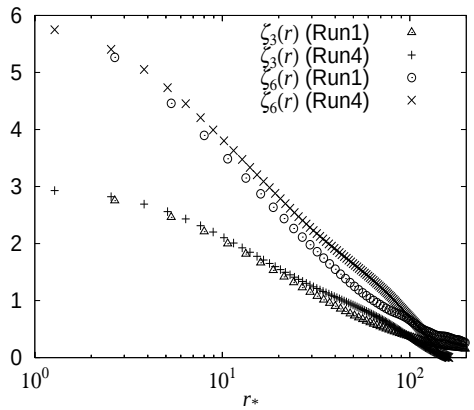

Fig. 8. The plot of the local slopes of $S_3(r)$ and $S_6(r)$ against r_* for Run 1 (decaying turbulence) and Run 4 (forced turbulence). The power-law dependence is not appreciable.

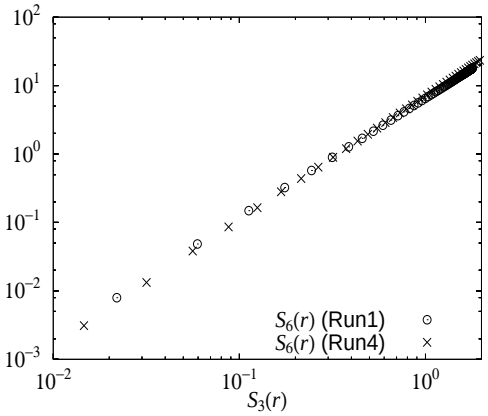

Fig. 9. The plot of $S_6(r)$ against $S_3(r)$ for Run 1 (decaying turbulence) and Run 4 (forced turbulence). Here the power-law dependence is appreciable.

5.1 Decaying turbulence

In this section, we will employ the local slope method, which has the advantage that it requires less care in choosing where to draw the appropriate straight fitting-line on the graph. In Fig. 10 the local slope of $\log S_n(r)$ of Run 1 is depicted. Note that the abscissa in this plot is not $\log S_3(r)$, but $\log r_*$, which is determined from $S_3(r)$. It is remarkable that all the local slopes take on constant values in the interval $16.0 \le r_* \le 29.4$. This indicates that the scaling determined here is reliable. Runs 2 and 3, using different Reynolds numbers and different realizations, have almost the same exponents as Run 1, although the scaling-range differs slightly from case to case. The local slopes ζ_n for Runs 1 to 3 are listed in Table II along with the scaling ranges. The last entry in the table shows the standard numbers fitted by an SL model.[3] Observe that when the Reynolds number increases, ζ_2 increases while $\zeta_n, (n \ge 4)$ decreases. The measured exponents in the decaying turbulence simulations are slightly (but definitely) less than the standard numbers obtained in forced turbulence studies.

We will now turn to a discussion of the condition of isotropy and the extent of non-stationarity in connection with the determination of the exponents of structure function. The isotropic conditions for the second- and third-order structure functions are guaranteed in the scaling range. We will now seek a connection with the non-stationarity of the functions. Such effects are inferred from the study of the KHK equation, or equivalently, from the third-order structure function. The KHK relation of Run 1 (Fig. 4) shows that the effect of the non-stationarity term $\partial D_{LL}(r)/\partial t$ is not negligible in the scaling range $16.0 \le r_* \le 29.4$, which is the range in which the scaling exponents of the structure functions for Run 1 are satisfactorily obtained. Study of the results reveals that the non-stationary effect is 22.4% of the $(4/5)\overline{\varepsilon}r$ at $r_* = 29.4$, which is the upper cutoff, while it is only 8.2% at $r_* = 16.0$. If the non-stationary effect is included in the total interaction, the energy flux in the scale-space of r is

$$\varepsilon(r) \equiv \overline{\varepsilon}\left(1 + \frac{15}{4\overline{\varepsilon}r^5}\int_0^r \frac{\partial D_{LL}(r',t)}{\partial t} r'^4 \mathrm{d}r'\right), \qquad (5.5)$$

which can be derived from eq. (4.5). Since the integrand of the second term on the right-hand side of the above equation is negative in decaying turbulence, it follows that the function $\varepsilon(r)$ decreases as r increases.

In order to see the effect of non-stationarity on higher-order structure functions, it is useful to examine the equation for the $n+1$th moment of the increment of the ith velocity component $w_i = u_i(\boldsymbol{x}_2) - u_i(\boldsymbol{x}_1)$, which is derived in Appendix A as eq. (A·7). It is:

$$\frac{\partial}{\partial r_k}\langle w_k w_i^n\rangle + n\left\langle w_i^{n-1}\frac{\partial}{\partial X_i}\delta p(\boldsymbol{X},\boldsymbol{r},t)\right\rangle = G_n^{(i)}(\boldsymbol{r}) - D_n^{(i)}(\boldsymbol{r}) + 2\nu\nabla_{\boldsymbol{r}}^2\langle w_i^n\rangle, \qquad (5.6)$$

where $G_n^{(i)}$ represents the non-stationarity effect

$$G_n^{(i)}(\boldsymbol{r}) = -\frac{\partial}{\partial t}\langle w_i^n\rangle, \qquad (5.7)$$

and $D_n^{(i)}$ expresses the correlation of the dissipation rate and w_i^n, which is written:

$$D_n^{(i)}(\boldsymbol{r}) = 2n(n-1)\left\langle \varepsilon_i(\boldsymbol{X},\boldsymbol{r}) w_i^{n-2}\right\rangle. \qquad (5.8)$$

Here ε_i is the dissipation rate of the kinetic energy of the ith velocity component at the two points $\boldsymbol{X} \pm \boldsymbol{r}/2$. It is written:

$$\varepsilon_i(\boldsymbol{X},\boldsymbol{r}) = \frac{\nu}{4}\left[|\nabla_{\boldsymbol{X}} w_i|^2 + 4|\nabla_{\boldsymbol{r}} w_i|^2\right] = \frac{\nu}{2}\left[|\nabla u_i(\boldsymbol{X}+\boldsymbol{r}/2)|^2 + |\nabla u_i(\boldsymbol{X}-\boldsymbol{r}/2)|^2\right]. \qquad (5.9)$$

A weighted energy flux can then be written as

$$\left\langle \varepsilon_i(\boldsymbol{X},\boldsymbol{r}) w_i^{n-2}\right\rangle [1 - \rho_n^{(i)}(\boldsymbol{r})], \qquad (5.10)$$

where

$$\rho_n^{(i)}(\boldsymbol{r}) = -\frac{1}{2n(n-1)}\frac{\frac{\partial}{\partial t}\langle w_i^n\rangle}{\left\langle \varepsilon_i(\boldsymbol{X},\boldsymbol{r}) w_i^{n-2}\right\rangle}. \qquad (5.11)$$

Since $\varepsilon_i(\boldsymbol{X},\boldsymbol{r})$ is positive-definite, as can be established from its definition (5.9), and the PDF for w_i is negatively skewed, then the denominator in $\rho_n^{(i)}(\boldsymbol{r})$ is positive for even n and negative for odd n. On the other hand, the numerator is negative for even n, and positive for odd n, because its amplitude decreases with time for decaying turbulence. Thus $\rho_n^{(i)}(\boldsymbol{r})$ is a positive quantity. The weighted flux is thus smaller than the value without the inclusion of the non-stationarity effect. Therefore it is possible that the non-stationarity effect yields a different scaling for the structure functions in question.

Although the KHK equation was not computed for Runs 2 and 3 (because the data for the time derivative were not stored during measurement), we can estimate the effect of non-stationarity by comparing the term $D_{LLL} - 6\nu\partial D_{LL}/\partial r$ to $-(4/5)\overline{\varepsilon}r$, since the effect of decay is attributed to their difference. To save on space in this paper, we do not include this figure in the text, but we have noticed that the non-stationarity effect is not negligible in Runs 2 and 3 where larger Reynolds-number values are exhibited.

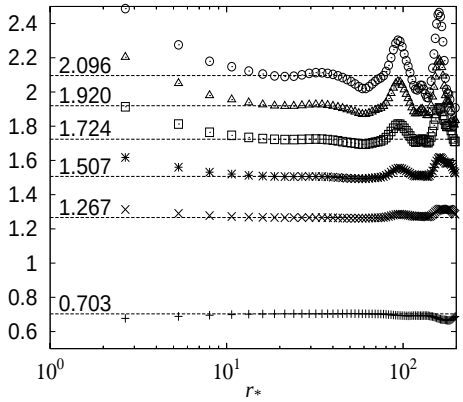

Fig. 10. The local slopes of the structure functions for Run 1; pluses stand for ζ_2, crosses for ζ_4, stars for ζ_5, squares for ζ_6, triangles for ζ_7, and circles for ζ_8. The straight dotted lines are drawn with numbers averaged over the scaling region.

	Run 1	Run 2	Run 3	Run 4	Run 5	SL
condition	decay	decay	decay	forced	forced	
fitting region r_*	$16.0 \sim 29.4$	$11.7 \sim 26.0$	$12.4 \sim 48.0$	$11.5 \sim 28.1$	$10.2 \sim 30.6$	
ζ_2	0.703	0.705	0.713	0.690	0.692	0.696
ζ_4	1.266	1.264	1.252	1.288	1.284	1.280
ζ_5	1.507	1.502	1.477	1.555	1.546	1.548
ζ_6	1.724	1.718	1.680	1.804	1.788	1.778
ζ_7	1.920	1.915	1.864	2.037	2.011	2.001
ζ_8	2.096	2.095	2.035	2.254	2.217	2.211

Table II. Scaling Exponents. The last entry, denoted as SL, shows the standard values presented in ref. 3.

5.2 Forced turbulence

We will now discuss the structure functions for Run 4 averaged over 126 samples for approximately 50 eddy-turnover times. The calculated local slopes have been plotted against r_* and are shown in Fig. 11. The constancy of the slopes in the interval $11.5 \le r_* \le 28.1$ is extremely impressive. Although the Reynolds number is 70, the exponents are very close to the standard values. Run 5, which has a flow of even higher Reynolds number, yields similar results, as can be seen in Table II. Note that the scaling range is rather narrow in Run 5, despite its larger Reynolds number, than in Run 4. We suspect that the reason for this is that the sample number is not large enough in Run 5, where we averaged over only 9 eddy turnover times, compared to the 50 eddy turnover times used in Run 4. In accord with current understanding of the process, we see that longer runs yield wider scaling ranges.

We will now investigate the connection between isotropy and external forcing. Note that for the scaling region used for this test, the isotropic conditions are well satisfied, while the KHK equation is affected slightly by the external-forcing terms. According to Fig. 5, the effect of external forces is small in the above scaling range. However, careful inspection of the numerical results shows that the forcing term in KHK is 13.3% of $(4/5)\overline{\varepsilon}r$ at $r_* = 28.1$ and 2.3% at $r_* = 11.5$. This reveals that external forcing does not affect the lower inertial region, which is where the constant local slopes begin, but some effect is evident in the upper inertial region.

In forced turbulence, the equation for the $n+1$th moment of the increment takes the form:

$$\frac{\partial}{\partial r_k}\langle w_k w_i^n\rangle + n\left\langle w_i^{n-1}\frac{\partial}{\partial X_i}\delta p(\boldsymbol{X},\boldsymbol{r},t)\right\rangle = H_n^{(i)}(\boldsymbol{r}) - D_n^{(i)}(\boldsymbol{r}) + 2\nu\nabla_{\boldsymbol{r}}^2\langle w_i^n\rangle, \quad (5.12)$$

where $H_n^{(i)}$ represents the contribution of the external force, and is written as

$$H_n^{(i)}(\boldsymbol{r}) = \frac{1}{9}n(n-1)\varepsilon_{in}(k_e r)^2\langle w_i^{n-2}\rangle. \quad (5.13)$$

(See Appendix A for a more complete explanation of this term.) The importance of the external forces can then be estimated through the ratio of $H_n^{(i)}(\boldsymbol{r})$ to the transfer term on the left-hand side of eq. (5.12):

$$\frac{H_n^{(i)}(\boldsymbol{r})}{\frac{\partial}{\partial r_k}\langle w_k w_i^n\rangle} \sim (k_e r)^2 r^{\alpha_n},$$

where $\alpha_n = 1 + \zeta_{n-2} - \zeta_{n+1}$, is an increasing function of n and approaches the constant value 2/3, according to the SL model. This estimate predicts that the influence of the external forces will diminish as the order of the structure function increases. Consequently, the effect of the external forces will not be significant in the higher-order structure functions.

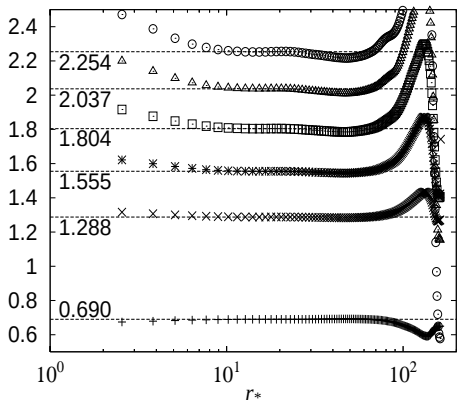

Fig. 11. The local slopes of the structure functions for Run 4. The plus symbols represent ζ_2, the crosses ζ_4, the stars ζ_5, the squares ζ_6, the triangles ζ_7, and the circles ζ_8. The straight dotted lines are drawn with numbers averaged over the scaling region.

5.3 Comparison

The results of our careful simulations show the scaling exponents to be definitely smaller in the decaying turbulence simulations than in the forced turbulence simulations. Recently, Boratav and Pelz[8] obtained the scaling indices for simulation of decaying turbulence with $R_\lambda = 82$, which agrees with the standard values. However, they did not employ a method of computing the local slope of the structure functions and identifying the scaling region with the constant local slope. They simply drew a best-fit line on their graphed curve to estimate its slope. Such a method will predict a different set of scaling indices depending on which region is chosen.

Let us now consider the reasons why the exponents are smaller for decaying turbulence than for forced turbulence. One conceivable reason for this phenomenon is that it is caused by the effect of the system's non-stationarity, as discussed in §5.1. One may argue that large Reynolds number flows do not suffer from non-stationarity effects; however, since the magnitude of the

non-stationarity effects decreases only by a certain power law as r decreases, the entire inertial region should be affected by the influence of non-stationarity.

Another possible reason for this discrepancy is that the dissipative structure may be different in decaying turbulence than in forced turbulence. Quantitatively,

$$\left\langle \varepsilon_i(\boldsymbol{X},\boldsymbol{r}) w_i^{n-2} \right\rangle \tag{5.14}$$

may scale differently in decaying- and forced-turbulence environments. As is shown in Appendix B, the pressure gradient term in eq. (5.6) is not affected by fluctuations at a far distance, and it obeys the same scaling relationship as the inertial term. Hence the left-hand side of eq. (5.6) is represented primarily by the inertial term. The essential equation for the inertial range is

$$(1+I_{n-1}^{(i)})\frac{\partial}{\partial r_k}\langle w_k w_i^n\rangle = -2n(n-1)\left\langle \varepsilon_i(\boldsymbol{X},\boldsymbol{r}) w_i^{n-2}\right\rangle, \tag{5.15}$$

where $I_{n-1}^{(i)}$ represents the contribution from the pressure gradient (see Appendix B). If the fluctuation of the dissipation rate is neglected, then the above equation can be replaced by:

$$(1+I_{n-1}^{(i)})\frac{\partial}{\partial r_k}\langle w_k w_i^n\rangle = -\frac{2}{3}n(n-1)\bar{\varepsilon}\left\langle w_i^{n-2}\right\rangle, \tag{5.16}$$

which governs the K41 scaling. In real turbulence however, the dissipation rate fluctuates in such a way that $[w_i(\boldsymbol{X},r)]^{n-2}$ and $\varepsilon_i(\boldsymbol{X},\boldsymbol{r})$ are positively correlated. Under these circumstances we have intermittent scaling, where the scaling exponents are smaller than their K41 values.

It is possible that the correlation of $[w_i(\boldsymbol{X},r)]^{n-2}$ and $\varepsilon_i(\boldsymbol{X},\boldsymbol{r})$ differs for decaying turbulence and forced turbulence. This may happen because the dissipative structure differs for the two turbulences and the non-stationarity effect may also affect the correlation (5.14). Precise analysis of the smaller exponents in decaying turbulence is a topic left for future study.

§6. Finite Reynolds Number Effect on the Scaling Exponents

So far, we have computed the structure functions for decaying and forced turbulence using a statistically sufficient number of samples, and have estimated the scaling exponents using the ESS method. In this section, we discuss the behavior of the structure function. If one looks at the plot of the structure function against $\log r_*$ (as for $\log S_6(r)$ in Fig. 7, for example,) it can be seen that the curve's shape may be approximated in the scaling region by a quadratic form of $\log r_*$:

$$\log S_n(r) = A_n + B_n \log r_* - \frac{C_n}{2}(\log r_*)^2. \tag{6.1}$$

Here A_n, B_n and C_n are positive. Note that as the Reynolds number, R_λ, increases, the linear range of the above equation increases, indicating that C_n decreases with R_λ. From the results of our studies, we suspect that B_n varies little with changes in R_λ. The local exponents can then be computed from

$$\zeta_n(r) = B_n - C_n \log r_*. \tag{6.2}$$

As r_* increases, the structure functions saturate (that is, become independent of r), as can be seen from the plot of $S_6(r)$ in Fig. 7. This implies that $\zeta_n(r)$ goes to zero at the saturation scale. We then require that $\zeta_n(r)=0$ at $r=L_0$. Note that we do not necessarily think that L_0 is the same as the external length. Consequently,

$$\log\frac{L_0}{\eta} = \frac{B_n}{C_n} = \text{const} \equiv M, \tag{6.3}$$

and substituting eq. (6.3) into eq. (6.2) yields

$$\zeta_n(r) = B_n\left(1-\frac{\log r_*}{M}\right). \tag{6.4}$$

Since C_n decreases with R_λ, M will increase with R_λ. Employing the ESS expression $\zeta_n = \zeta_n(r)/\zeta_3(r)$, eq. (6.4) leads us to

$$\zeta_n = \frac{B_n(1-\log r_*/M)}{B_3(1-\log r_*/M)} = \frac{B_n}{B_3}, \tag{6.5}$$

which is independent of r_*, so long as we stay in the scaling range. This explains why the ESS works so well for our simulations. In the limit of infinite R_λ, $B_3 \to 1$ and therefore, $B_n \to \zeta_n$.

We will now discuss the evidence supporting eq. (6.4), relying on our present simulations and other experiments employing large Reynolds numbers. Figure 12 shows a plot of the local slopes $\zeta_n(r)$ against r_* for Run 4, in which various straight lines fitted in the inertial region (where the scaling exponents are to be determined) are extrapolated outside of the scaling region. All the lines converge to a single point, $(10^M, \zeta_n = 0)$, although the data points for large r_* values are suppressed to emphasize the convergence. The relation (6.4) is remarkably well satisfied with $M = \log 143 = 2.16$. Other runs with forced turbulence show the same tendency with $M = \log 188 = 2.27$ for Run 5. It is clear from these results that M increases as R_λ increases. For the decaying turbulence of Run 1 using the same R_λ as Run 4, $M = \log 112 = 2.05$ which is slightly smaller than the corresponding value for Run 4. This is interpreted as likely being due to a possibly larger C_n value for decaying turbulence resulting from the non-stationarity effect.

The linearity of $\zeta_n(r)$ with respect to $\log r_*$ is demonstrated in experiments for turbulent flows with Reynolds numbers larger than the present study.[16,20] It should be noted though that the scale ranges where the linearity holds in these experiments are located at larger scale values than in our studies. Note that the local slopes are shown for more restricted values of n in those other experiments; for example: $M = \log 2\times 10^5 = 5.28$ in the flow of $R_\lambda = 2000$,[20] where M is read from the plot of $\zeta_6(r)$ (see Fig. 2(d) in ref. 20). According to the flow of $R_\lambda = 19500$,[16] $M \sim 11$ is estimated from $\zeta_2(r)$ (from Fig. 4(a) in ref. 16), and $M \sim 10$ from $\zeta_6(r)$ (from Fig. 4(b) in the same publication). In order to see how M varies with R_λ, we create a log-log plot of M against R_λ, as in Fig. 13. From this we can establish the rough relationship: $M \sim R_\lambda^{0.3}$. We expect this relationship to be confirmed in future work.

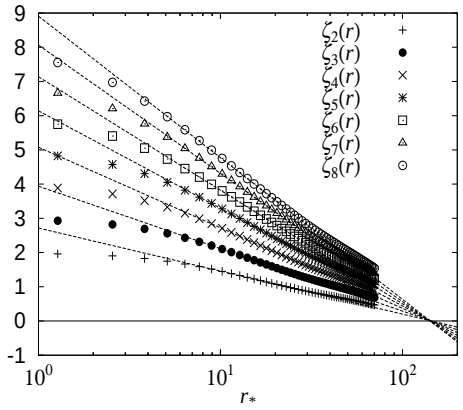

Fig. 12. The verification of relation (6.4) for Run 4. The data points for large values of r_* are suppressed to emphasize that the scaling lines converge to a single point at $(r_* = 143, \zeta_n = 0)$.

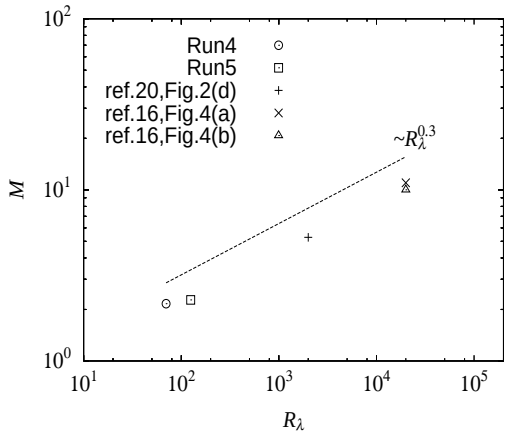

Fig. 13. The curve of M against R_λ. A circle symbol represents the data for Run 4, and a square the data for Run 5. A plus indicates the data for the experiment of $R_\lambda = 2000$,[20] and a cross (derived from $\zeta_2(r)$) and a triangle (derived from $\zeta_6(r)$) show the results for experiments of $R_\lambda = 19500$.[16] The broken line represents the relation $M \sim R_\lambda^{0.3}$.

§7. Summary and Discussion

In this paper we have examined turbulence conditions to accurately determine the longitudinal structure function through the incompressible expressions of the second- and third-order structure functions and through the KHK relation. The examination of the isotropy for the second- and third-order structure functions, in terms of the incompressibility conditions, showed that the isotropy of these functions is well satisfied when averages are taken over the ensemble of the initial field or over a sufficient period. It was found that the non-stationarity effect due to the decaying and forcing effects penetrates into the upper inertial range, and the ESS method must be applied to measure the scaling exponents of the structure functions on scales smaller than those of penetration.

The degree of anisotropy of turbulent flow will increase with the order of the structure function, as can be inferred from our observation that the third-order structure function is more anisotropic than the second-order function. The problem lies in determining to what extent the anisotropy affects the higher-order structure functions. It is difficult to numerically predict the anisotropic effects, because the simple expressions for the isotropy of such systems, as related in eqs. (3.1) and (3.2), have not yet been extended to include the higher-order structure functions. Also, we do not yet know how the effect of non-stationarity changes with the order of the structure functions. This could possibly be estimated by examining numerically the factor defined in eq. (5.11).

We have computed the scaling indices of the structure functions up to the eighth order, which we believe to be the maximum order for which accurate results are given under the above considerations. It was found that the exponents are definitely smaller for decaying turbulence than for forced turbulence. Further studies are necessary, however, to derive definite conclusions either extending or disproving this observation for turbulence with higher-order structure functions. Our limited current results for simulated decaying turbulence, however, do indeed show the smaller numbers.

Since smaller exponents correspond to the more intermittent characteristics in the turbulence, we see that decaying turbulence is more intermittent than forced turbulence. It is widely recognized that a coherent structure with a very large velocity gradient is of the form of a vortical tube which has a diameter and length of the order of the Kolmogorov- and integral-lengths. It is plausible that random forcing at a large scale acts to destroy the coherence of such a structure over the integral scale. On the other hand, in decaying turbulence there is no such mechanism to prevent the development of a coherent structure in the velocity field, other than basic restrictions imposed by the computational box-size or experimental geometry. For this reason, we observe that decaying turbulence is more intermittent than the forced variety.

We have argued that the local-scaling exponents $\zeta_n(r)$ can be expressed as a linear function of $\log r_*$, reflecting the finite nature of the Reynolds number. When the Reynolds number becomes large, the correction term arising from the effect of the finite Reynolds number vanishes.

Acknowledgements

The work of T.G. and T.N. presented here was supported by a Grant-in-Aid for Scientific Research (C) 09640260 from The Ministry of Education, Science, Sports and Culture of Japan, and by RIKEN. We are grateful to T. Ochiai at NIT for his assistance in the numerical computation involved in this work.

Appendix A: Derivation of Karman-Howarth-Kolmogorov Equation

Although the derivation of the KHK equation is given in most standard books dealing with turbulence,[11] we will derive this equation for a structure function of arbitrary order and will include the effects of forcing. Note that the KHK equation turns out to be nothing more than the equation for the second-order structure function.

Let $\boldsymbol{u}_1$ and $\boldsymbol{u}_2$ be the velocity of the flow at locations

$\boldsymbol{x}_1$ and $\boldsymbol{x}_2$. The average velocity $\boldsymbol{V}$ and the relative velocity $\boldsymbol{w}$ are defined as

$$\boldsymbol{w}(\boldsymbol{x}_2,\boldsymbol{x}_1)=\boldsymbol{u}_2-\boldsymbol{u}_1,\quad \boldsymbol{V}=(\boldsymbol{u}_2+\boldsymbol{u}_1)/2.$$

The equation for $\boldsymbol{w}$ is derived by taking the difference of the Navier-Stokes equations at $\boldsymbol{x}_2$ and $\boldsymbol{x}_1$;

$$\begin{aligned}&\frac{\partial}{\partial t}\boldsymbol{w}(\boldsymbol{x}_2,\boldsymbol{x}_1)+(\boldsymbol{u}_2\cdot\nabla_2+\boldsymbol{u}_1\cdot\nabla_1)\boldsymbol{w}(\boldsymbol{x}_2,\boldsymbol{x}_1)\\&=-\left(\frac{\partial}{\partial\boldsymbol{x}_2}+\frac{\partial}{\partial\boldsymbol{x}_1}\right)(p(\boldsymbol{x}_2)-p(\boldsymbol{x}_1))\\&\quad+\nu(\nabla_2^2+\nabla_1^2)\boldsymbol{w}(\boldsymbol{x}_2,\boldsymbol{x}_1)+\boldsymbol{f}(\boldsymbol{x}_2)-\boldsymbol{f}(\boldsymbol{x}_1),\end{aligned}\quad\text{(A·1)}$$

where $\boldsymbol{f}$ is an external random Gaussian force, p is the pressure and ν is the kinematical viscosity. Notice that the variable $\boldsymbol{x}_2$ is held constant when the partial derivative with respect to $\boldsymbol{x}_1$ is taken, and similarly for $\boldsymbol{x}_1$ when the partial derivative with respect to $\boldsymbol{x}_2$ is taken. Now, we introduce the quantities

$$\boldsymbol{X}=(\boldsymbol{x}_1+\boldsymbol{x}_2)/2,\quad \boldsymbol{r}=\boldsymbol{x}_2-\boldsymbol{x}_1.$$

Since

$$\frac{\partial}{\partial\boldsymbol{x}_1}=\frac{1}{2}\frac{\partial}{\partial\boldsymbol{X}}-\frac{\partial}{\partial\boldsymbol{r}},\quad \frac{\partial}{\partial\boldsymbol{x}_2}=\frac{1}{2}\frac{\partial}{\partial\boldsymbol{X}}+\frac{\partial}{\partial\boldsymbol{r}},$$

we are led to the expressions:

$$\begin{aligned}\boldsymbol{u}_2\cdot\nabla_2+\boldsymbol{u}_1\cdot\nabla_1&=\boldsymbol{V}(\boldsymbol{X},\boldsymbol{r},t)\cdot\nabla_{\boldsymbol{X}}+\boldsymbol{w}(\boldsymbol{X},\boldsymbol{r},t)\cdot\nabla_{\boldsymbol{r}},\\\nabla_2+\nabla_1&=\nabla_{\boldsymbol{X}},\\\nabla_2^2+\nabla_1^2&=\frac{1}{2}\nabla_{\boldsymbol{X}}^2+2\nabla_{\boldsymbol{r}}^2.\end{aligned}$$

Here $\boldsymbol{w}(\boldsymbol{X},\boldsymbol{r})$ is the velocity difference $\boldsymbol{w}(\boldsymbol{x}_1,\boldsymbol{x}_2)$ with a change of variables from $\boldsymbol{x}_1$, $\boldsymbol{x}_2$ to $\boldsymbol{X}$, $\boldsymbol{r}$.

On substituting the above relations into eq. (A·1), the Navier-Stokes equation for the velocity difference becomes

$$\begin{aligned}&\left(\frac{\partial}{\partial t}+V_k(\boldsymbol{X},\boldsymbol{r},t)\frac{\partial}{\partial X_k}\right)w_i(\boldsymbol{X},\boldsymbol{r},t)\\&=-w_k(\boldsymbol{X},\boldsymbol{r},t)\frac{\partial}{\partial r_k}w_i(\boldsymbol{X},\boldsymbol{r},t)-\frac{\partial}{\partial X_i}\delta p(\boldsymbol{X},\boldsymbol{r},t)\\&\quad+\nu\left(\frac{1}{2}\nabla_{\boldsymbol{X}}^2+2\nabla_{\boldsymbol{r}}^2\right)w_i(\boldsymbol{X},\boldsymbol{r},t)+\delta f_i(\boldsymbol{X},\boldsymbol{r},t),\end{aligned}\quad\text{(A·2)}$$

where

$$\begin{aligned}\delta p(\boldsymbol{X},\boldsymbol{r},t)&=p(\boldsymbol{x}_2,t)-p(\boldsymbol{x}_1,t),\\\delta\boldsymbol{f}(\boldsymbol{X},\boldsymbol{r},t)&=\boldsymbol{f}(\boldsymbol{x}_2,t)-\boldsymbol{f}(\boldsymbol{x}_1,t).\end{aligned}$$

Note that the following incompressible condition

$$\begin{aligned}\frac{\partial}{\partial\boldsymbol{X}}\cdot\boldsymbol{V}&=\frac{1}{2}\frac{\partial}{\partial\boldsymbol{X}}\cdot(\boldsymbol{u}(\boldsymbol{x}_2)+\boldsymbol{u}(\boldsymbol{x}_1))\\&=\frac{1}{2}\left(\frac{\partial}{\partial\boldsymbol{x}_2}\cdot\boldsymbol{u}(\boldsymbol{x}_2)+\frac{\partial}{\partial\boldsymbol{x}_1}\cdot\boldsymbol{u}(\boldsymbol{x}_1)\right)=0,\end{aligned}$$

holds, because $\boldsymbol{r}$ is held constant when the partial derivative with respect to $\boldsymbol{X}$ is taken. Similarly,

$$\frac{\partial}{\partial\boldsymbol{X}}\cdot\boldsymbol{w}=\frac{\partial}{\partial\boldsymbol{r}}\cdot\boldsymbol{V}=\frac{\partial}{\partial\boldsymbol{r}}\cdot\boldsymbol{w}=0.$$

Multiplying eq. (A·2) by w_i^{n-1}, and reorganizing the dissipation term slightly, we get

$$\begin{aligned}&\frac{1}{n}\frac{\partial}{\partial t}w_i^n+\frac{1}{n}\boldsymbol{V}(\boldsymbol{X},\boldsymbol{r},t)\cdot\nabla_{\boldsymbol{X}}w_i^n\\&=-\frac{1}{n}\boldsymbol{w}\cdot\nabla_{\boldsymbol{r}}w_i^n-w_i^{n-1}\frac{\partial}{\partial X_i}\delta p(\boldsymbol{X},\boldsymbol{r},t)\\&\quad+\frac{\nu}{2}\nabla_{\boldsymbol{X}}\cdot(w_i^{n-1}\nabla_{\boldsymbol{X}}w_i)+\frac{2}{n}\nu\nabla_{\boldsymbol{r}}^2w_i^n\\&\quad-2(n-1)\varepsilon_i(\boldsymbol{X},\boldsymbol{r})w_i^{n-2}+\delta f_iw_i^{n-1}.\end{aligned}\quad\text{(A·3)}$$

Here,

$$\begin{aligned}\varepsilon_i(\boldsymbol{X},\boldsymbol{r})&=\frac{\nu}{4}\left[|\nabla_{\boldsymbol{X}}w_i|^2+4|\nabla_{\boldsymbol{r}}w_i|^2\right]\\&=\frac{\nu}{2}\left[|\nabla u_i(\boldsymbol{X}+\boldsymbol{r}/2)|^2+|\nabla u_i(\boldsymbol{X}-\boldsymbol{r}/2)|^2\right]\end{aligned}\quad\text{(A·4)}$$

is the summation of the energy-dissipation rate of the ith component of the velocity field at the two points $\boldsymbol{x}_1$ and $\boldsymbol{x}_2$.

Let us now calculate the correlation of δf_i and w_i^{n-1}, which appears in eq. (A·3),

$$F_i(n)=\left\langle\delta f_i(t)w_i^{n-1}\right\rangle_f,$$

where $\langle\cdot\rangle_f$ signifies the average over Gaussian random forces. Since the random force is simply delta correlated in time, and $\delta f_i(s)(s\le t)$ correlates with $\delta f_i(t)$ only at $t=s$, it is appropriate to use the approximation

$$w_i(t)=\int_{-\infty}^{t}\delta f_i(s)\mathrm{d}s$$

in the computation of the correlation $\left\langle\delta f_i(t)w_i^{n-1}\right\rangle_f$. Substituting this result into one of the $n-1$ components of w_i, we have

$$F_i(n)=(n-1)w_i^{n-2}\int_{-\infty}^{t}\langle\delta f_i(t)\delta f_i(s)\rangle_f\mathrm{d}s.$$

In the present simulation, external forces are added randomly, once per time-step Δt, so that

$$F_i(n)=(n-1)w_i^{n-2}\left\langle\delta f_i^2\right\rangle_f.$$

The correlation of random forces is calculated through

$$\begin{aligned}\left\langle\delta f_i^2\right\rangle_f&=\sum_{\boldsymbol{k},\boldsymbol{q}}\langle f_i(\boldsymbol{k})f_i(\boldsymbol{q})\rangle_f\mathrm{e}^{i(\boldsymbol{k}+\boldsymbol{q})\cdot\boldsymbol{X}}\\&\quad\times\left(\mathrm{e}^{i\boldsymbol{k}\cdot\boldsymbol{r}/2}-\mathrm{e}^{-i\boldsymbol{k}\cdot\boldsymbol{r}/2}\right)\left(\mathrm{e}^{i\boldsymbol{q}\cdot\boldsymbol{r}/2}-\mathrm{e}^{-i\boldsymbol{q}\cdot\boldsymbol{r}/2}\right)\\&=\sum_{\boldsymbol{k}}\langle f_i(\boldsymbol{k})f_i^*(\boldsymbol{k})\rangle_f(1-\mathrm{e}^{-i\boldsymbol{k}\cdot\boldsymbol{r}})(1-\mathrm{e}^{i\boldsymbol{k}\cdot\boldsymbol{r}})\\&=2\sum_{\boldsymbol{k}}\left\langle|f_i(\boldsymbol{k})|^2\right\rangle_f(1-\cos\boldsymbol{k}\cdot\boldsymbol{r}),\end{aligned}$$

where the homogeneity of the system is employed. Since the random forces are limited to wavenumbers smaller than $1/r$, where r is our scale of interest, $\cos\boldsymbol{k}\cdot\boldsymbol{r}$ may be expanded in terms of $\boldsymbol{k}\cdot\boldsymbol{r}$. Furthermore, we can make use of the property that the external forces are distributed

in an isotropic way. Then

$$\left\langle \delta f_i^2 \right\rangle_f = \sum_{\boldsymbol{k}} \left\langle |f_i(\boldsymbol{k})|^2 \right\rangle_f (\boldsymbol{k}\cdot\boldsymbol{r})^2 = \frac{r^2}{3} \sum_{\boldsymbol{k}} \left\langle |f_i(\boldsymbol{k})|^2 \right\rangle_f k^2.$$

When we introduce the definition

$$k_e^2 = \frac{\sum_{\boldsymbol{k}} \left\langle |f_i(\boldsymbol{k})|^2 \right\rangle_f k^2}{\sum_{\boldsymbol{k}} \left\langle |f_i(\boldsymbol{k})|^2 \right\rangle_f},$$

we have

$$\left\langle \delta f_i^2 \right\rangle_f = \frac{1}{3}(k_e r)^2 \sum_{\boldsymbol{k}} \left\langle |f_i(\boldsymbol{k})|^2 \right\rangle_f.$$

Since the energy-input rate ε_{in} due to the external forces is

$$\varepsilon_{in} = 3\left\langle f_i^2 \right\rangle_f = 3 \sum_{\boldsymbol{k}} \left\langle |f_i(\boldsymbol{k})|^2 \right\rangle_f, \tag{A·5}$$

we are led to the relation

$$F_i(n) = \frac{1}{9}(n-1)\varepsilon_{in}(k_e r)^2 w_i^{n-2}. \tag{A·6}$$

Substituting eq. (A·6) into eq. (A·3) and taking the ensemble average over the velocity field, we have

$$\begin{aligned}\frac{\partial}{\partial t}\langle w_i^n \rangle = &-\frac{\partial}{\partial r_k}\langle w_k w_i^n \rangle - n\left\langle w_i^{n-1}\frac{\partial}{\partial X_i}\delta p(\boldsymbol{X},\boldsymbol{r},t)\right\rangle \\ &+2\nu\nabla_{\boldsymbol{r}}^2\langle w_i^n\rangle - 2n(n-1)\left\langle \varepsilon_i(\boldsymbol{X},\boldsymbol{r}) w_i^{n-2}\right\rangle \\ &+\frac{1}{9}n(n-1)\varepsilon_{in}(k_e r)^2\left\langle w_i^{n-2}\right\rangle. \end{aligned}\tag{A·7}$$

Note that we have not made the summation over i at this point.

Let us now focus on the KHK relation, which is derived by substituting $n = 2$ into eq. (A·7) and making the summation over i. We then have:

$$\begin{aligned}&\frac{\partial}{\partial t}\sum_i \langle w_i^2\rangle + \frac{\partial}{\partial r_k}\sum_i \langle w_k w_i^2\rangle \\ &= 2\nu\nabla_{\boldsymbol{r}}^2 \sum_i \langle w_i^2\rangle - 4\sum_i \langle \varepsilon_i(\boldsymbol{X},\boldsymbol{r})\rangle + \frac{2}{3}\varepsilon_{in}(k_e r)^2. \end{aligned}\tag{A·8}$$

Making use of the relations from [11]

$$\sum_i \langle w_i^2\rangle = \frac{1}{r^2}\frac{\partial}{\partial r} r^3 D_{LL},$$

$$\sum_i \langle w_k w_i^2\rangle = \frac{r_k}{3r^4}\frac{\partial}{\partial r} r^4 D_{LLL},$$

$$\sum_i \langle \varepsilon_i(\boldsymbol{X},\boldsymbol{r})\rangle = \overline{\varepsilon},$$

we arrive at

$$\begin{aligned}&\frac{1}{r^2}\frac{\partial}{\partial r} r^3 \frac{\partial}{\partial t} D_{LL} + \frac{1}{3r^2}\frac{\partial}{\partial r}\left[\frac{1}{r}\frac{\partial}{\partial r} r^4 D_{LLL}\right] \\ &\qquad = \frac{2\nu}{r^2}\frac{\partial}{\partial r}\left[\frac{1}{r}\frac{\partial}{\partial r} r^4 \frac{\partial}{\partial r} D_{LL}\right] - 4\overline{\varepsilon} + \frac{2}{3}\varepsilon_{in}(k_e r)^2. \end{aligned}$$

First, we multiply the above equation by $3r^2$, and then integrate it over r from 0 to r. Second, we multiply the result by r, and integrate it again over r. We then get

$$\begin{aligned}D_{LLL} = &-\frac{4}{5}\overline{\varepsilon} r + 6\nu\frac{\partial D_{LL}}{\partial r} \\ &-\frac{3}{r^4}\int_0^r \frac{\partial D_{LL}}{\partial t} r'^4 \mathrm{d}r' + \frac{2}{35}\varepsilon_{in}(k_e r)^2 r, \end{aligned}\tag{A·9}$$

for $(k_e r)^2 \ll 1$. Note that the last term on the right-hand side of (A·9), for arbitrary r, is given by:

$$\begin{aligned}&\frac{4\varepsilon_{in} r}{\sum_{\boldsymbol{k}} \langle |f_i(\boldsymbol{k})|^2\rangle} \sum_{\boldsymbol{k}} \langle |f_i(\boldsymbol{k})|^2\rangle \\ &\quad \times \left(\frac{1}{5} + \frac{3}{k^3 r^3}\sin kr + \frac{9}{k^4 r^4}\cos kr - \frac{9}{k^5 r^5}\sin kr\right). \end{aligned}\tag{A·10}$$

Appendix B: Contribution of the Pressure Gradient Term

The equation for the structure function of arbitrary-order has been derived above. Each term appearing in the equation acts locally in space except for the pressure-gradient term. The pressure is usually considered to be a long-ranged influence, because it is related to the far velocity-fields through the Poisson kernel. Consequently, the same is commonly thought to be true for pressure-gradient forces. Here we show that the pressure-gradient term is not as long-ranged as thought. The fact that the pressure-gradient term has a local nature was mentioned previously by L'vov and Procaccia,[14] but the argument can be better illustrated if we use the results in the Appendix A.

Let us take the divergence of eq. (A·2) with respect to X_i. Since the external forces are divergence-free, we are led to the equation:

$$\begin{aligned}\nabla_{\boldsymbol{X}}^2 \delta p(\boldsymbol{X},\boldsymbol{r},t) = -\frac{\partial}{\partial X_j}\Big[&w_k(\boldsymbol{X},\boldsymbol{r},t)\frac{\partial}{\partial r_k} w_j(\boldsymbol{X},\boldsymbol{r},t) \\ &+V_k(\boldsymbol{X},\boldsymbol{r},t)\frac{\partial}{\partial X_k} w_j(\boldsymbol{X},\boldsymbol{r},t)\Big]. \end{aligned}\tag{B·1}$$

The source term can be simplified as follows. The incompressibility condition reduces the source term to

$$-\frac{\partial w_k(\boldsymbol{X},\boldsymbol{r},t)}{\partial X_j}\frac{\partial w_j(\boldsymbol{X},\boldsymbol{r},t)}{\partial r_k} - \frac{\partial V_j(\boldsymbol{X},\boldsymbol{r},t)}{\partial X_k}\frac{\partial w_k(\boldsymbol{X},\boldsymbol{r},t)}{\partial X_j},$$

where the interchanging of $(j \leftrightarrow k)$ has been done in the second term. Since

$$\begin{aligned}\frac{\partial}{\partial X_k} V_j(\boldsymbol{X},\boldsymbol{r},t) &= \frac{1}{2}\frac{\partial}{\partial X_k}\left[u_j(\boldsymbol{X}+\boldsymbol{r}/2) + u_j(\boldsymbol{X}-\boldsymbol{r}/2)\right] \\ &= \frac{\partial}{\partial r_k}\left[u_j(\boldsymbol{X}+\boldsymbol{r}/2) - u_j(\boldsymbol{X}-\boldsymbol{r}/2)\right] \\ &= \frac{\partial}{\partial r_k} w_j(\boldsymbol{X},\boldsymbol{r},t), \end{aligned}$$

the source term becomes

$$\begin{aligned}&-2\frac{\partial w_k(\boldsymbol{X},\boldsymbol{r},t)}{\partial X_j}\frac{\partial w_j(\boldsymbol{X},\boldsymbol{r},t)}{\partial r_k} \\ &\qquad = -2\frac{\partial}{\partial X_j}\frac{\partial}{\partial r_k} w_k(\boldsymbol{X},\boldsymbol{r},t) w_j(\boldsymbol{X},\boldsymbol{r},t). \end{aligned}$$

The pressure-gradient term then reduces to:

$$\frac{\partial}{\partial X_i}\delta p(\boldsymbol{X},\boldsymbol{r}) = \int \mathrm{d}\boldsymbol{X}' K_{ij}(\boldsymbol{X},\boldsymbol{X}') \times \frac{\partial}{\partial r_k} w_k(\boldsymbol{X}',\boldsymbol{r},t) w_j(\boldsymbol{X}',\boldsymbol{r},t), \quad \text{(B·2)}$$

where

$$K_{ij}(\boldsymbol{X},\boldsymbol{X}') = \frac{1}{2\pi}\frac{\partial}{\partial X_i}\frac{\partial}{\partial X_j}\frac{1}{|\boldsymbol{X}-\boldsymbol{X}'|}. \quad \text{(B·3)}$$

The pressure-gradient term appearing in eq. (A·7) becomes

$$E_{n-1}(w_i(r)) \equiv n\left\langle w_i^{n-1}\frac{\partial}{\partial X_i}\delta p\right\rangle = n\int \mathrm{d}\boldsymbol{R} K_{i\alpha}(\boldsymbol{R}) B_\alpha^{(n-1)}(\boldsymbol{R},\boldsymbol{r},t), \quad \text{(B·4)}$$

$$B_\alpha^{(n-1)}(\boldsymbol{R},\boldsymbol{r},t) = \left\langle w_i^{n-1}(\boldsymbol{X},\boldsymbol{r},t)\frac{\partial}{\partial r_\beta} w_\beta(\boldsymbol{X}+\boldsymbol{R},\boldsymbol{r},t) \times w_\alpha(\boldsymbol{X}+\boldsymbol{R},\boldsymbol{r},t)\right\rangle, \quad \text{(B·5)}$$

where the summation is taken only over the repeated Greek variables, and $K_{ij}(\boldsymbol{R})$ is a dipole-type interaction:

$$K_{ij}(\boldsymbol{R}) = \frac{1}{2\pi R^3}\left[3\frac{R_i R_j}{R^2} - \delta_{ij}\right]. \quad \text{(B·6)}$$

The average value (B·5) does not contain the following contribution,

$$\left\langle w_i^{n-1}(\boldsymbol{X},\boldsymbol{r},t)\right\rangle\left\langle \frac{\partial}{\partial r_\beta} w_\beta(\boldsymbol{X}+\boldsymbol{R},\boldsymbol{r},t) w_\alpha(\boldsymbol{X}+\boldsymbol{R},\boldsymbol{r},t)\right\rangle,$$

since the latter average vanishes due to the fact that the divergence of the second-order structure function is zero. Therefore, the two quantities at $\boldsymbol{X}$ and $\boldsymbol{X}+\boldsymbol{R}$, that is:

$$w_i^{n-1}(\boldsymbol{X},\boldsymbol{r},t) \quad \text{and} \quad \frac{\partial}{\partial r_\beta} w_\beta(\boldsymbol{X}+\boldsymbol{R},\boldsymbol{r},t) w_\alpha(\boldsymbol{X}+\boldsymbol{R},\boldsymbol{r},t)$$

must be correlated. It is certain that such a correlation function must decrease with increasing separation $\boldsymbol{R}$ for $R \geq r$.

For $|\boldsymbol{r}|$ in the inertial range, the integral of eq. (B·4) may be written as

$$\left(\int_{R<r} \mathrm{d}\boldsymbol{R} + \int_{R>r} \mathrm{d}\boldsymbol{R}\right) K_{i\alpha}(\boldsymbol{R}) B_\alpha^{(n-1)}(\boldsymbol{R},\boldsymbol{r}). \quad \text{(B·7)}$$

The first integral, $B_\alpha^{(n-1)}(\boldsymbol{R},\boldsymbol{r})$, can be Taylor-expanded in $|R/r|$ as

$$B_\alpha^{(n-1)}(\boldsymbol{R},\boldsymbol{r}) = B_\alpha^{(n-1)}(0,\boldsymbol{r}) + \nabla_{\boldsymbol{R}} B_\alpha^{(n-1)}(0,\boldsymbol{r})\cdot\boldsymbol{R} + \cdots. \quad \text{(B·8)}$$

When this form is substituted into the first integral of eq. (B·7), the first term of eq. (B·8) vanishes due to the symmetry of the system:

$$\int \mathrm{d}\boldsymbol{R}\frac{1}{2\pi R^3}\left[3\frac{R_i R_j}{R^2} - \delta_{ij}\right] = 0.$$

The other terms will make their contributions mostly around $R \sim r$.

Examining the second integral in eq. (B·7), we may reasonably assume that the correlation $B_\alpha^{(n-1)}(\boldsymbol{R},\boldsymbol{r})$ behaves as $(R/r)^{-\delta}$, for $R/r > 1$ with $\delta > 0$. Thus the contribution from the upper boundary of the second integral of eq. (B·7) can be neglected, because

$$\int \mathrm{d}\boldsymbol{R}\frac{1}{2\pi R^3}\left[3\frac{R_i R_j}{R^2} - \delta_{ij}\right] R^{-\delta} \to 0 \qquad \text{as } R\to\infty. \quad \text{(B·9)}$$

Since this integral is dominated by scales of R comparable to r, $B_\alpha^{(n-1)}(\boldsymbol{R}=\boldsymbol{r},\boldsymbol{r})$ can be approximated as a homogeneous function of r,

$$B_\alpha^{(n-1)}(r\boldsymbol{\nu},\boldsymbol{r}) \approx r^\phi L_\alpha^{(n-1)}(\boldsymbol{\nu},\boldsymbol{\mu}),$$

where $\boldsymbol{\nu} = \boldsymbol{R}/R, \boldsymbol{\mu} = \boldsymbol{r}/r$ and $L_\alpha^{(n-1)}(\boldsymbol{\nu},\boldsymbol{\mu})$ is a geometric function of $\boldsymbol{\nu}$ and $\boldsymbol{\mu}$. ϕ is the same as the scaling exponent of $\left\langle w_i^{n-1}\frac{\partial}{\partial r_\beta} w_\beta w_\alpha\right\rangle$.

Now $E_{n-1}(w_i(r))$ can be evaluated as

$$E_{n-1}(w_i(r)) \approx r^\phi n J_i^{(n-1)}(\boldsymbol{\mu}), \quad \text{(B·10)}$$

$$J_i^{(n-1)}(\boldsymbol{\mu}) = \frac{1}{2\pi}\int \mathrm{d}\Omega(\boldsymbol{\nu})\left(3\nu_i\nu_\alpha - \delta_{i\alpha}\right) L_\alpha^{(n-1)}(\boldsymbol{\nu},\boldsymbol{\mu}). \quad \text{(B·11)}$$

This development implies that the greatest contribution to the integrals (B·4) comes from the range of R comparable to r, meaning that the dominant contribution to the pressure-gradient term is from the near correlation on the order of $R \sim r$. As far as the scaling of the pressure-gradient term in r is concerned, the contribution from the pressure-gradient in eq. (A·7) obeys the same scaling as the inertial term $\frac{\partial}{\partial r_\alpha}\langle w_\alpha w_i^n\rangle$. We may then write:

$$E_{n-1}(w_i(r)) = I_{n-1}^{(i)}(\boldsymbol{\mu})\frac{\partial}{\partial r_\alpha}\langle w_\alpha w_i^n\rangle, \quad \text{(B·12)}$$

where $I_{n-1}^{(i)}$ is a function of the order one, depending on $\boldsymbol{\mu}$. The factor n on the right hand side of eq. (B·10) is absorbed into the exponent of $\frac{\partial}{\partial r_\alpha}\langle w_\alpha w_i^n\rangle$.

[1] A.S. Monin and A.M. Yaglom: *Statistical Fluid Mechanics*, volume II (MIT Press, Cambridge, Mass., 1973), W.D. McComb: *The physics of fluid turbulence* (Oxford University Press, New York, 1990), U. Frisch: *Turbulence* (Cambridge University Press, Cambridge, England, 1995).

[2] A.N. Kolmogorov: Dokl. Akad. Nauk. SSSR **30** (1941) 299.

[3] In order to see numerically how the exponents deviate from K41, refer to Z.S. She and E. Leveque: Phys. Rev. Lett. **72** (1994) 336.

[4] R. Camussi, D. Barbagallo, R. Guj and F. Stella: Phys. Fluids **8** (1996) 1181.

[5] R. Camussi and R. Benzi: Phys. Fluids **9** (1997) 257.

[6] B. Dhruva, Y. Tsuji and K.R. Sreenivasan: Phys. Rev. E **56** (1997) R4928.

[7] A. Noullez, G. Wallace, W. Lempert, R.B. Miles and U. Frisch: J. Fluid Mech. **339** (1997) 287.

[8] O.N. Boratav and R.B. Pelz: Phys. Fluids **9** (1997) 1400.

[9] S. Chen, K.R. Sreenivasan, M. Nelkin and N. Cao: Phys. Rev. Lett. **79** (1997) 2253.

[10] F. Moisy, P. Tabeling and H. Willaime: Phys. Rev. Lett. **82** (1999) 3994.

[11] A detailed presentation of this equation can be found in Monin and Yaglom in ref. 1, and T. Gotoh: *Fundamental Turbulence Theory* (Asakura, Tokyo, 1998) 1st ed., [in Japanese].

[12] R. Benzi, S. Ciliberto, R. Tripiccione, C. Baudet, F. Massailoli and S. Succi: Phys. Rev. E **48** (1993) R29.

[13] R. Benzi, S. Ciliberto, C. Baudet and G.R. Chavarria: Physica D **80** (1995) 385.
[14] V.S. L'vov and I. Procaccia: Phys. Rev. Lett. **77** (1996) 3541.
[15] A. N. Kolmogorov: Dokl. Akad. Nauk. SSSR **32** (1941) 1.
[16] K.R. Sreenivasan and B. Dhruva: Prog. Theor. Phys. Suppl. **130** (1998) 103.
[17] L. Danaila, F. Anselmet, T. Zhou and R.A. Antonia: J. Fluid Mech. **391** (1999) 359.
[18] G. Stolovitzky and K.R. Sreenivasan: Phys. Rev. E **48** (1993) R33.
[19] N. Cao, S. Chen and Z.S. She: Phys. Rev. Lett. **76** (1996) 3711.
[20] F. Belin, R. Tabling and H. William: Physica D **93** (1996) 52.
[21] S. Grossmann, D. Lohse and A. Reeh: Phys. Rev. E **56** (1997) 5473.